Master of Science Thesis

Digital Tomosynthesis: Fundamental principles and comparison to conventional X-ray imaging

Christian Bernhardsson

Supervisor: Anders Tingberg, PhD

The work has been performed at
Department of Radiation Physics
Malmö University Hospital

Medical Radiation Physics
Clinical Sciences, Lund
Lund University, 2006

Contents

Abstract

During the last century several attempts have been made to overcome the fundamental problem of X-ray imaging, i.e. that anatomical information existing in 3-dimensions has to be represented on a 2-dimensional radiograph. In this thesis, digital tomosynthesis, a refined version of conventional tomography, has been investigated. Digital tomosynthesis enables retrospective reconstruction of an arbitrary plane in the imaged patient from a series of low dose projections, acquired with a limited tube movement. In the simplest method of reconstructing arbitrary planes, all the projections are shifted such that structures from only one plane line up exactly and thus remain fixed relative to the over- and underlying structures. To investigate the fundamental principles of tomosynthesis and evaluate the clinical potential a prototype was built. Quality metrics such as signal difference to noise ratio (SDNR) and artifact spread function (ASF) were measured with different tomographic parameter settings. The tomosynthesis acquisition parameters were optimized and the image quality at different exposure levels were compared to conventional radiographs. The optimization evaluation showed that a large angular range with many projections can increase the image quality and reduce artifacts created from surrounding anatomy. It was also shown that small and obscured objects were easier to discern with tomosynthesis compared to conventional X-ray imaging, even at lower exposures. Reconstructed images of an anthropomorphic chest phantom showed an increased visibility of local structures in the lungs, structures which becomes superimposed on surrounding anatomy in a conventional X-ray image. These results are a consequence of the intrinsic property of tomosynthesis; each image, reconstructed from a series of projections, have high signal from in-focus objects and low signal from the surrounding anatomy that is repeated over the image proportional to the number of projections. The ability to separate the surrounding anatomy from the in-focus structures can be optimized with the appropriate combination of angular range and the number of projections acquired.

1 Introduction

The X-ray modalities clinically available today include 2-dimensional imaging (i.e. planar imaging, geometrical tomography, mammography, angiography and fluoroscopy) and 3-dimensional imaging (computed tomography, CT). In a conventional X-ray image all structures in the imaged 3D volume become superimposed onto a 2D radiograph. This can decrease the ability for the radiologist to detect pathologies and therefore lead to inaccurate diagnoses. Geometrical tomography is limited to high-contrast imaging [1] but is a low cost alternative to CT and reduces the confusion of over- and underlying structures by focusing on one specific plane. In geometrical tomography the entire thickness of the patient is exposed to acquire a single tomogram (slice). If several slices are needed to locate the lesion, multiple exposures are required and the dose to the patient will increase proportional to the number of slices acquired. The 3D imaging modality, CT, is a complex X-ray technique that utilizes the ideas of tomography with the aid of computers to make 2D slices of 3D objects. CT images has undoubtedly led to significant advances in patient care, although high levels of patient dose are involved and it is expensive to implement.

In this paper another X-ray modality will be investigated, namely digital tomosynthesis. This is a 3D imaging technique that has the ability to address some of the shortcomings of the other X-ray modalities. Digital tomosynthesis reduces the confusion of superimposed structures and allows retrospective reconstruction of an arbitrary number of tomographic planes, at a lower cost and lower dose than CT.

The principles of tomosynthesis are not new but have evolved from geometrical tomography. Geometrical tomography [2] was first implemented by Ziedses des Plantes 1932 after several other attempts [3]. Not until 1969 when Garison *et al.* made a successful experiment [4] the first tomosynthesis images were seen. Since the pioneers were using film-based systems [5] [6], the post processing of the images was limited. Another disadvantage which did not make tomosynthesis clinically acceptable in the beginning was the lengthy procedure with a film change between each exposure. To shorten the tomosynthesis acquisition time video cameras coupled to an image intensifier screen and a television display were utilized [7]. Later the analogue video cameras became digital with the introduction of the charge-coupled device (CCD). Then it was possible to acquire higher quality X-ray images and store them digitally. The only problem left was the lack of computational power needed for the reconstruction. In the late 1970s the introduction of tomosynthesis as a new modality seemed to have failed, when CT became widely accepted. The further development of tomosynthesis was then slow until the late 1990s when rapid digital flat-panel detectors became available and the cost of computing the tomosynthesis reconstruction and post-processing routines dropped. These technological advancements started a new interest in refining and developing tomosynthesis.

For a dedicated tomosynthesis equipment there are a few requirements that must be fulfilled;

- A large area digital detector capable of fast readout
- Because each exposure is low dose it is essential that the image receptor has a high detective quantum efficiency with low quantum- and electronic noise
- The system must be able to handle fast movement of the tube, in small and precise angle increments
- A fairly fast computer with reconstruction software

Today, detectors that fulfill these conditions are available and a tomosynthesis study can be

performed very fast, the whole series of projections can be acquired within a single breathhold [8] [9] (chest imaging). Tomosynthesis prototypes have been developed for mammography [10] and chest imaging [11] but several other imaging tasks are also investigated i.e. angiography, urography, images of inner ear, orthopedic, finger joints and dental applications [12]. Apart from clinical implementations of tomosynthesis much of the research is concentrated on developing new reconstruction algorithms and methods to reduce the blurring from out-of-plane structures. In this paper the fundamental properties of tomosynthesis as a new modality will be investigated. This includes parameters that will affect the final slices and a comparison to conventional X-ray imaging.

1.1 Theory

In conventional planar X-ray imaging there are a few factors that limit the ability to visualize structures, especially when they are small and obscured. One of the most fundamental factors is that objects in the imaged 3D volume become *superimposed* on the 2D radiograph. The data in each pixel is related to the sum of the different attenuation coefficients along the beam through the object, see equation 1. This will lower the contrast and make it difficult, or even impossible, to detect subtle anomalies. Another difficulty in planar imaging is that the spatial distribution of objects is obscured. This *geometrical effect* makes it hard to draw conclusions about the shape and relative position of various structures. A third factor, which contradictively is the factor that give rise to the contrast in the X-ray images, might also decrease the diagnostic information, is caused by *attenuation effects*. This effect arises from the fact that the incident X-ray intensity, I_0, reduces to I when striking the detector due to attenuation of the different organs. If a narrow beam of monoenergetic photons with an initial transmitted intensity, I_0, penetrating several tissues, i, of different thickness, x_i, and attenuation coefficients, μ_i, the intensity striking the detector, I, is given by the equation:

$$I = I_0 \cdot e^{-\sum_i \mu_i x_i} \tag{1}$$

From this equation it is easy to see that the beam attenuation, I/I_0, depends on both μ and x. This can cause uncertainties when comparing two structures that appears to be similar in an image. The structures might appear similar but can be composed of different tissues with different thickness since a difference in attenuation can be due to changes in thickness, composition or a combination of both.

1.1.1 Geometrical tomography

One method to overcome the previously described problems is with geometrical tomography, also called body tomography or conventional tomography. This method utilizes geometrical focusing techniques to achieve the tomographic effect. The word "tomography" comes from the Greek tomos (slice) and graphia (picture). The aim of tomographic imaging is to get a high contrast in one specific plane, the 'focal plane' or 'plane of cut', of the imaged object and blur out object structures outside of this layer. This can be accomplished by moving the tube and the detector, during a continuous emission of X-rays, provided that the middle of the tube always points at a specific position on the detector. The most common way to achieve this is to use a parallel-path geometry and move the tube and detector in a linear fashion, in opposite directions, as in figure 1.

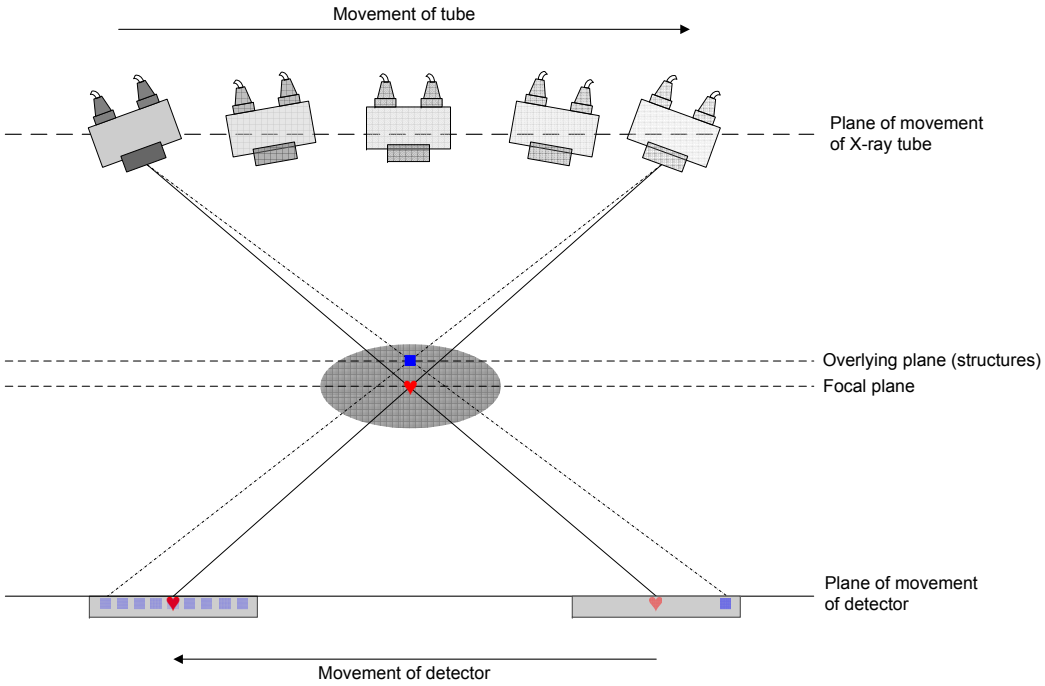

Figure 1: An illustration of linear tomography. When the exposure begins the tube is tilted, typically 20°, from the normal to the detector. During the exposure, continuous reinforcement of the structures in the focal plane (♡) is achieved while structures above this plane (■) is smeared out from right to left across the detector.

To do a geometrical tomography a focal plane must be selected, which will be the fulcrum of the system and this plane will determine the different speeds[1] of the tube and detector during the exposure. During the movement, continuous reinforcement of the focal plane is achieved while structures from over and underlying planes are blurred out due to parallax, proportional to their distance from the focal plane. Hence, in this geometry all objects in the focal plane will be projected to the same location on the detector and therefore, they appear to be stationary.

Since the out-of-plane anatomy of the patient is not efficiently removed from the image, tomographic images tend to be inherently low in contrast. Therefore, conventional tomography is used for high-contrast situations only, such as urography with contrast agents and imaging of the inner ear where the contrast is high between air to bone [1]. Another disadvantage is that only one plane per exposure can be set as the focal plane.

[1] When the focal plane is set in the middle of the X-ray tube and the detector, the tube and detector will move with the same speed and distance to the image volume.

1.1.2 Tomosynthesis

Tomosynthesis is similar to conventional geometrical tomography in that it uses the same geometry, the difference is the synthesis of the images. In tomosynthesis a sequence of projection radiographs are acquired during a single motion of the X-ray tube. These different radiographs allows for an arbitrary number of in-focus planes to be generated retrospectively. There are a few different geometrical configurations available for tomosynthesis [13] and the method proposed here is based on a linear movement of the tube-detector system.

In linear tomosynthesis the X-ray tube and detector move in opposite directions parallel to the fulcrum plane, see figure 2. Several low dose exposures are acquired during the movement from 1 to 3 and the tomographic angle (or angular range), ϕ, typically varies from -20$\leq \phi \leq$20 degree in intervals of about $\Delta\phi = 2$ degree, depending on the examination and system capabilities. The angle is from the perpendicular to the detector and the synchronous movement depends on where the fulcrum plane is situated (plane B in figure 2).

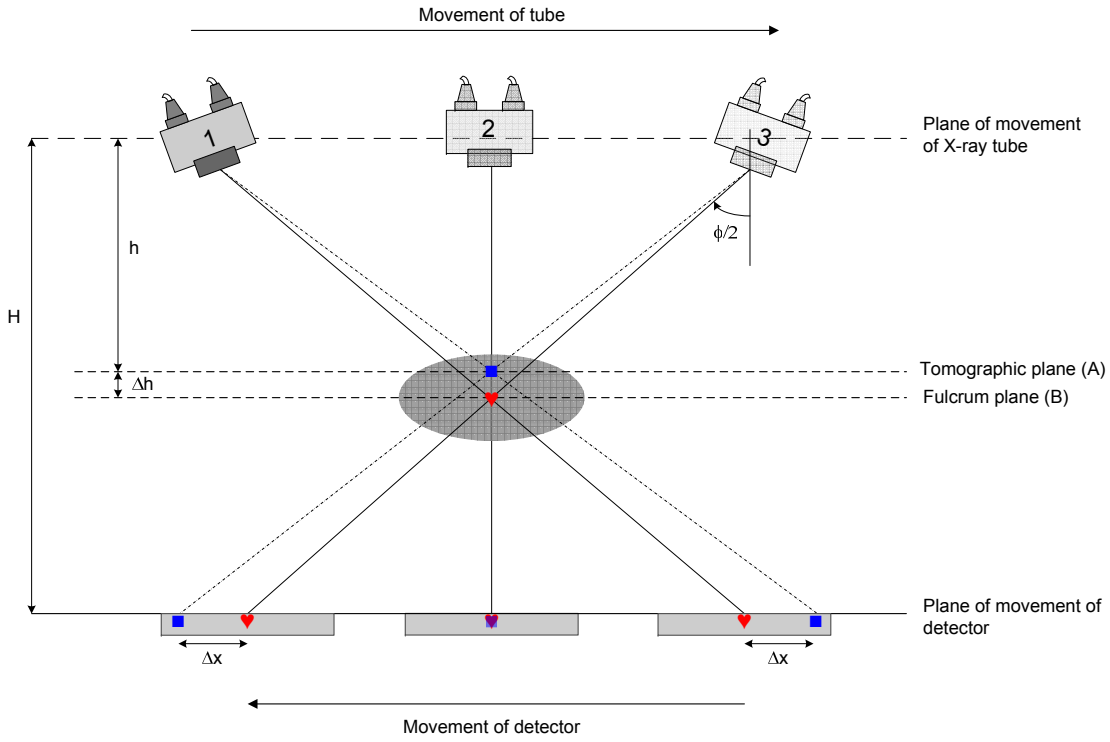

Figure 2: Illustration of the tube and detector movement during the tomographic motion (only three exposures are shown for simplicity). Plane B is the fulcrum plane separated Δh from the overlying plane, A. At the outermost projections (1 and 3) the object in plane A is displaced a specific amount Δx from the underlying object in plane B.

As in geometrical tomography the image structures in one plane are enhanced, the focal plane, and objects outside of this plane are blurred out if the different projections are just added. However, with a reconstruction method any plane through the volume can be set as the focal

plane, retrospectively. Several methods have been proposed for suppressing nonrelevant plane information and enhancing the image quality [14] - [18] but the most common is the so called 'Shift-And-Add' method [5] first proposed by *Grant*.

The Shift-And-Add method is akin to (unfiltered) backprojection and takes into consideration that objects at different heights above the detector will experience different degrees of parallax as the tube moves. When using linear geometry, the tube and detector move in synchrony in parallel planes so that the magnification of objects depends only on their height above the detector, not on the location of the tube or detector within these two planes. When these conditions are fulfilled it is possible to shift and add the different images to bring a specific plane into focus. During the first step, the images are shifted. The amount of shift, Δx, depends on the position of, and height above the detector. Consider the triangles created by the rays in figure 2. It is easy to se that the sides opposite to $\frac{\phi}{2}$ (parallel to the plane of movement of the tube) is given by

$$\Delta h \cdot \tan\frac{\phi}{2} + h \cdot \tan\frac{\phi}{2} \quad \text{and} \quad h \cdot \tan\frac{\phi}{2} \tag{2}$$

for the two smaller triangles and

$$\Delta x + H \cdot \tan\frac{\phi}{2} \quad \text{and} \quad H \cdot \tan\frac{\phi}{2} \tag{3}$$

for the other two. By similar triangles, the ratios of these sides must be equal, we get

$$\frac{\Delta h \cdot \tan\frac{\phi}{2} + h \cdot \tan\frac{\phi}{2}}{h \cdot \tan\frac{\phi}{2}} = \frac{\Delta x + H \cdot \tan\frac{\phi}{2}}{H \cdot \tan\frac{\phi}{2}} \tag{4}$$

The exact length of the shift, Δx, can then be calculated by regrouping eq. 4:

$$\Delta x = \frac{H \cdot \Delta h \cdot \tan\frac{\phi}{2}}{h} \tag{5}$$

were H is the focus-to-detector distance, h the distance from the tomographic plane (i.e. in-focus plane) and the tube, Δh the distance between the fulcrum- and tomographic plane (the plane to reconstruct) and ϕ is the tomographic angle. The projections are then added with the right amount of shift applied, so that the structures in plane A are all made to line up exactly and thus be in focus. In figure 3 the principles of the Shift-And-Add method is illustrated for the specific case in figure 2.

1.2 Purpose of the study

The purpose of this study was to evaluate the clinical potential of tomosynthesis and investigate if it was possible to obtain more information for a certain situation than conventional X-ray imaging at the same or even smaller dose. To determine this the different parameters associated with the acquisition and reconstruction processes had to be investigated and optimized.

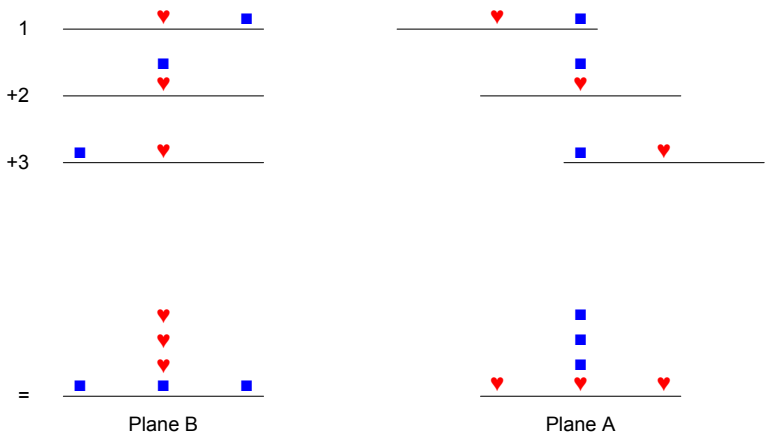

Figure 3: Tomosynthesis reconstruction method Shift-And-Add with three different projections. The focal plane (B) is brought to focus simply by adding the projections. Plane A is reconstructed by shifting the bilateral projections the same amount and adding them together with the middle projection.

2 Material and methods

The clinical interest in tomosynthesis is increasing but no dedicated system was available at Malmö University Hospital when this project was performed. Therefore, existing equipment was used to build a prototype, which included a Varian X-ray tube with a Canon CXDI (a-Si) digital flat panel detector and a computer. The Canon CXDI utilized a Large Area New MIS Sensor and TFT (LANMIT) with an image matrix of 2688×2688 pixels and a pixel pitch of 160 μm. The detector had a read-out of 0.3 seconds [20], which was considerably shorter than the time between each X-ray exposure (∼20 seconds).

The X-ray equipment was located at the urography section of the Radiology Department where the systems are capable of geometrical tomography. Hence, it was possible to use the geometrical configuration described in figure 1, however the X-ray unit was limited to an angular range of 60° (±30°). Since the system software only used the radiated part of the detector, each projection had a different matrix size. This is unacceptable when shifting and adding the projections since there is no fixed reference point. Thus, the system was modified by adjusting the software and force it to use a fix detector matrix for each projection. For every measurement a 2688×2688 pixel matrix was used with a 45×45 cm FOV, which was necessary because of the large phantoms used.

2.1 Phantoms

The phantoms used in the study included an abacus-like physical phantom (see figure 4) and an anthropomorphic chest phantom. The physical phantom was used to study the impact of different tomographic parameters on the reconstructed slices and in a comparative study with conventional X-ray imaging. The anthropomorphic chest phantom was investigated with both tomosynthesis and conventional X-ray imaging to compare the diagnostic value between the modalities.

The physical phantom frame is made of plexiglas (PMMA) and has the exterior dimensions: 300×190×140 mm. Inside the phantom there are several nylon strings (diameter of 1.5 mm) attached to the frame. The strings are placed to build up 4 different planes with 4 strings per plane. These planes will be refereed to as the "natural planes" to avoid confusion. The interspacing between the natural planes and also between the bottom of the phantom to the first plane is 30 mm. Spheres and ellipsoids of various sizes are attached to the strings (diameter of 30, 20, 15, 10, 7 and 5 mm). The spheres are made of polypropylene ($\rho = 0.910$ g/cm^3) and the ellipsoids of PMMA ($\rho = 1.190$ g/cm^3). To make the situation more realistic the phantom was filled with water. This small difference in density, compared to water ($\rho \approx 1$ g/cm^3), made the phantom optimal for a comparison study of conventional X-ray imaging and tomosynthesis.

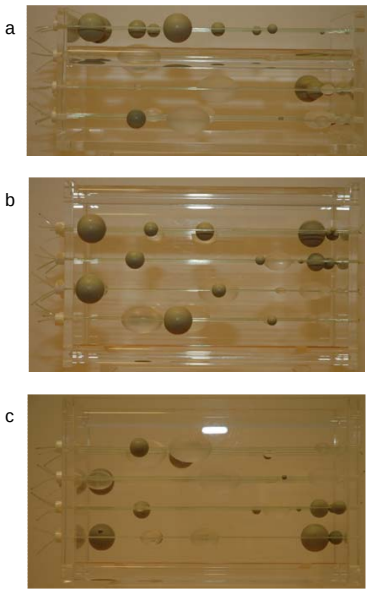

Figure 4: The physical phantom seen from; a) the side, b) above and c) below.

2.2 Image acquisition

In the physical phantom the different spheres and ellipsoids were movable. This made it possible to move and place different sized objects at interesting positions. In table 1, objects at the same position parallel to the detector plane (XY-plane) but different positions in the Z-direction are listed. These positions were chosen to obtain almost every possible arrangement

of the objects (overlying/underlying, size, composition, distance) and this configuration was utilized during the entire study. Since this will generate a large amount of data only some of the objects were investigated in close detail.

Table 1: The position of the spheres and ellipsoids in the different planes of the phantom. Each row in the table represents objects at the same XY-position but at heights above the table (Z-position).

Object	Size/mm	Depth/mm	Over-/Underlying object	Size/mm	Depth/mm
PMMA	15	30	Polyp.	15	120
PMMA	20	30	Polyp.	20	90
PMMA	30	30	Polyp.	30	120
Polyp.	5	30	PMMA	7	90
Polyp.	20	30	PMMA	30	90
PMMA	7	60	Polyp.	20	120
PMMA	30	60	Polyp.	15	120
PMMA	20	90	Polyp.	10	120
PMMA	10	90	Polyp.	10	120

Each acquisition was performed in the same manner. The phantom was placed on the table in the middle of the X-ray field, which was maximized (45×45 cm) to cover the entire phantom for every angle. The fulcrum plane (i.e. pivot for the movement of the tube and detector) was selected with a laser positioning system attached to the wall and coupled to the X-ray unit. This plane was selected in the middle of the phantom, 185 mm above the detector. When the positioning of the fulcrum plane was satisfactory, the phantom was filled with water (approx. 9.5 liters) and the position on the table adjusted, if it was necessary. Finally, the X-ray tube settings were configured and the acquisition could start. During the acquisition the X-ray tube was moved manually between each exposure and the precision of the angles depended on the built-in measuring device. A separate inclinometer was used to improve the accuracy of the measured angles from the built-in device to a precision of $\pm 1^{\circ}$. Nevertheless, the accuracy of the angles is not a crucial factor due to the inherent properties of the reconstruction method.

Because objects outside the slice of interest will appear as blurring artifacts in the tomosynthesis images and become superimposed on the conventional radiographs a CT study was also performed. Images reconstructed with a CT only contain information from the exposed slice, these images will therefore serve as a reference when comparing tomosynthesis to conventional X-ray imaging. For this purpose a Siemens Somatom Sensation 64 was utilized. A thorax routine protocol with 120 kV, 100 mAs and 3.2 mm slice thickness was used in this study. Since the reconstructed images were slices perpendicular to the table a special reconstruction program, In-space [21] had to be utilized. In-space offers the ability to reconstruct and view any plane throughout the imaged volume. With this tool the four natural planes of the phantom were located and saved, see figure 5.

2.3 Post-processing of the image data

After each acquisition the images were stored in the Picture Archiving and Communications Systems (PACS) and downloaded to a PC (P4 3.0 GHz and 1 Gb RAM) were the reconstruc-

tion was performed. The tomograms were synthesized from the projections with a software, based on the shift-and-add method, written in IDL [22]. The projections were not linearized (logarithmic transformed) prior to the reconstruction. A nonlinear relationship may be used to reconstruct images but will not be capable of removing blur from the images with deblurring algorithms. Here the tomosynthesis images were studied without such algorithms and therefore the blur in the images is determined by the tomographic parameters and the exposure will not be linearly related to the response on the detector.

In the tomosynthesis process there are a few variables in the reconstruction program that will affect the quality of the final slices. Therefore, some of the parameters together with the main parts of the program will be described.

During image acquisition, the projection of the object onto the detector moves/shifts laterally as the detector and X-ray source are moved with respect to each other. To reconstruct the object, the projection images are shifted with respect to each by incremental amounts and summed to obtain slices through the object. In order to avoid exceeding the dimensions of the detector field-of-view while shifting the images, a central region of interest is selected from the detector array. This region is restricted by an upper- and a lower limit, in the direction of the tube movement, determined by the total matrix height, number of slices necessary to cover the whole volume, the shift factor and which image that represented the 0°-projection.

Each of the projection images was read sequentially into the reconstruction program, with the 0°-projection (AP) in the middle. These were then rebinned to 672×672 pixels (1/16 of the original), to save computational time and a central region of interest selected, as described above. Each of the re-scaled images (except the one in the middle) were shifted and added to create a 3D volume of the slices. The specific amount of shift applied to the different projections depends on two factors; 1) the projection to shift and 2) the wanted in-focus plane. To create slices of the imaged volume from the series of projections a fixed shift factor was introduced, which typically varied between 0.05 to 0.2 pixels and determines the distance between two adjacent slices. Depending on the reconstruction depth (or the wanted in-focus plane) the shift factor was weighted accordingly to the two factors above. In this way it is possible to generate an unlimited number of slices, for a given series of projections. However, the resolution will not increase infinitely but will be restricted by the point-spread function (PSF) of the system.

When all of the projection images had been shifted and added to bring a specific plane into focus the new images, i.e. slices, were stored as .tiff files (16-bit grayscale) for analysis with an image viewer. To find the right planes for investigation, a volume rendering was created which gave a gross estimate on where the slices were cutting the phantom. For each situation every third slice were stored and when the best in-focus slice was located among these, the closest over- and underlying planes were studied further.

2.4 Tomographic parameters

The first investigation was to determine how the tomographic parameters affect the reconstructed slices. The examined parameters included the tomographic angle, ϕ, angle increment between each projection, $\Delta\phi$, and the number of acquired projections, N_{Acq}. Because $N_{Acq} = \frac{\phi}{\Delta\phi} + 1$ it is impossible to fix two of them and vary the third. Therefore the study of the tomographic parameters was divided into three cases. For each case a specific parameter was fixed to cover all possible situations. The settings used for each case is listed in table 2.

When the phantom was placed on the table and filled with water, the X-ray tube settings were configured. This was done by changing kilovoltage and mAs to get a good image quality in a 0° AP-projection. At 60 kVp and 105 mAs the signal from the different objects was high enough to discern most of the objects in the phantom. The tube loading were then divided among the projections in the tomosynthesis series so that the total exposure was the same.

When all projections in the series were acquired a 3D volume was reconstructed using a software written in IDL and slices cutting the natural planes of the phantom were saved. The quality of the images were evaluated by both a visual comparison and measurement of the signal difference to noise ratio (SDNR) for six of the smallest objects in the phantom. The measurements were made in the middle of the objects and in the adjacent background. In order to do the comparison more consequent ROIs were placed so that no part of them were located in an artifact. The SDNR is a measure of the detectability of an object in a reconstructed plane and is defined by

$$SDNR = \frac{\bar{\mu}_{object} - \bar{\mu}_{BG}}{\sigma_{BG}} \tag{6}$$

were $\bar{\mu}_{object}$ is the mean pixel intensity of the object, $\bar{\mu}_{BG}$ is the mean intensity of the image background, and σ_{BG} is the standard deviation of the homogenous background pixel intensity calculated in a large ROI with ImageJ [23]. The ROIs were placed at the same position in the objects and in the image background so that no part of the ROIs were located in an artifact.

When the different parameters associated with the acquisition vary, artifacts caused by over- and underlying structures will also vary. The artifacts appear as blur in the reconstructed slices and will reduce the diagnostic value of the images. To quantify the magnitude of the blur an artifact spread function (ASF) [24] was utilized. This is an extension of the PSF which is a measure of the spread of signal of a point. The ASF is a measure of the intensity of the artifact relative to the intensity of the (real) object causing the artifact. Another way to interpret the ASF is the capability of tomosynthesis in differentiating objects that are superimposed along the Z direction, the direction perpendicular to the reconstruction plane (XY). The ASF is defined by

$$ASF(z) = \frac{\bar{\mu}_{artifact}(z) - \bar{\mu}_{BG}(z)}{\bar{\mu}_{object}(z_0) - \bar{\mu}_{BG}(z_0)} \tag{7}$$

were $\bar{\mu}_{artifact}(z)$ and $\bar{\mu}_{BG}(z)$ are the mean pixel intensities of the artifact and the background in the off-focus plane z, $\bar{\mu}_{object}(z_0)$ and $\bar{\mu}_{BG}(z_0)$ are the mean pixel intensities of the object and the image background in the in-focus plane z_0, respectively. The ASF was measured for the 30 mm polypropylene sphere located at plane 4 (z_0 = 120 mm above the table). $\bar{\mu}_{object}(z_0)$ was measured with a ROI placed over the (real) object in plane four and a ROI in the image background measured $\bar{\mu}_{BG}(z_0)$. In every fourth plane, between plane 4 to plane

Table 2: Parameter settings for the investigation of the tomographic parameters.

Case	ϕ	$\Delta\phi$	N_{Acq}
1	20°, 40°, 60°	2°, 4°, 6°	11
2	40°	2°, 4°, 5°,	21, 11, 9
3	20°, 40°, 60°	2°	11, 21, 31

1 at z = 30 mm above the table, the intensity of the artifact (the numerator in equation 7) was measured. The ROI to measure $\bar{\mu}_{artifact}(z)$ was placed over the region of the artifact at the same position in all of the slices and with the same area. The image background in the off-focus planes, $\bar{\mu}_{BG}(z)$, was measured with a ROI outside the artifact.

2.5 Tomosynthesis compared to conventional X-ray imaging

2.5.1 Exposure

To do a comparison study between the modalities, images acquired with the conventional technique were compared to tomosynthesis images acquired with the same mAs and kVp. Five 0°-projections or anterior-posterior (AP) projections were acquired at 60 kVp and different mAs. The tomosynthesis examination were performed with the same, or as close as possible to the total exposure (mAs), of the conventional AP. The tomosynthesis examination (TS) included 11 projections over an angular range of 40°. In table 3 the different settings for each comparison are listed.

Table 3: The different mAs settings for the AP and the associated TS projections. For each case the difference of the total mAs between the methods are listed, with AP projection as reference.

Study	Conventional/mAs	mAs per tomosynthesis proj.	Total difference/%
1	32	3.1	10
2	64	6.2	6
3	128	12.5	10
4	252	20.0	-8
5	400	32.0	-8

When comparing the five studies, three different objects within the phantom were selected. These included a 15 mm PMMA ellipsoid ($z = 30$ mm above the table), a 20 mm polyprophylene sphere ($z = 30$ mm above the table) and a 10 mm polyprophylene sphere ($z = 120$ mm above the table). The objects were selected since they were the smallest objects visible in all of the images and had different properties (size, composition, over-/underlying structures). At each mAs-setting the SDNR were measured for these three objects and compared between the techniques.

2.5.2 Anthropomorphic phantom

To investigate the clinical benefits of tomosynthesis an anthropomorphic chest phantom was studied with conventional radiography and tomosynthesis. The phantom was positioned in an AP view mode and the scanning direction along the spine with an angular range of 20° and 2° steps. A conventional chest image is typically acquired with 140 kVp and 2 mAs but it was not possible to generate such high kVp/mAs ratio due to the tube rating, therefore 100 kVp and 3.2 mAs were used instead.

To define the location of the slices, two fiducial markers were placed on a ruler at different positions above the table, $z_{up} = 150$ mm and $z_{low} = 50$ mm and there were N_{recon} reconstructed slices evenly spread between z_{up} and z_{low}. The reconstructed planes were located

at $z_i = z_{low} + i \cdot \Delta z$, were $0 \leqslant i \leqslant N_{recon} - 1$ and Δz is a measure of the distance between the slices, defined by

$$\Delta z = \frac{z_{up} - z_{low}}{N_{recon} - 1} \tag{8}$$

The clinical information obtained from the tomosynthesis acquisition was visually compared to that from the conventional.

3 Results

As reference or gold standard, images of the physical phantom acquired with CT are enclosed in figure 5. In these images it is possible to see all of the structures in the phantom as well as the nylon strings.

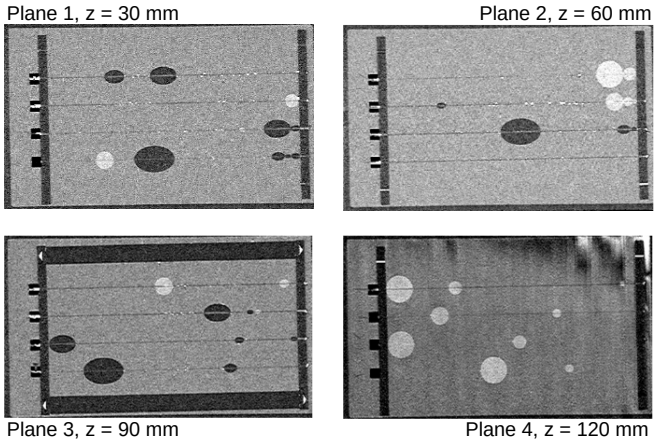

Figure 5: The four natural planes of the physical phantom acquired with CT. Because the objects within the physical phantom were loose there are some small differences between the tomosynthesis slices and the CT slices although the objects positions in the Z-direction are retained.

3.1 Tomographic parameters

Some illustrative examples from the different cases are shown in figure 6. As the angular range increases, out-of-plane objects are smeared over a larger area and therefore appear with diminished intensity compared with objects in focus. This effect is possible to see in figure 6 where the smeared object is marked with an arrow.

The images acquired with the conventional technique and tomosynthesis were compared and the SDNR was measured for some of the smallest objects in the phantom, see figure 7. A large angular range seems to lower the SDNR and in some of the images it was not possible to see the objects (with $\phi = 60°$). Figure 7C indicate that a large number of projections

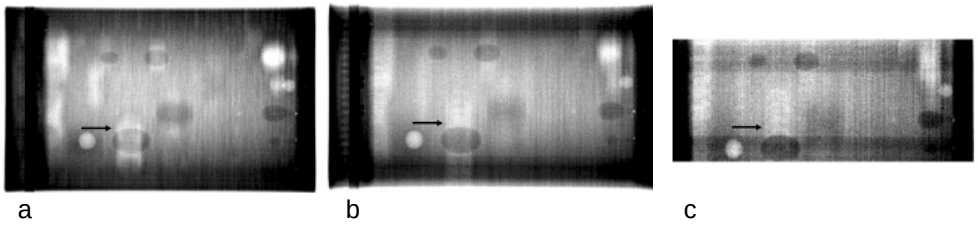

Figure 6: Examples of plane 1 in the physical phantom, reconstructed from projections acquired with; a) $\phi = 20°$ and $\Delta\phi = 2°$, b) $\phi = 40°$ and $\Delta\phi = 4°$, c) $\phi = 60°$ and $\Delta\phi = 6°$. Objects in overlying planes becomes more smeared out (marked with an arrow) when ϕ and $\Delta\phi$ increases. This increases the visibility of the structures in the in-focus plane. Note that the images have different sizes due to the increase in number of shifts, not the increase in angle.

with a small angular range will improve the SDNR. In figure 7B it is not possible to see any relationship between $\Delta\phi$ and the SDNR when the angular range is fixed and the angle increment is varied.

The effect of the blurring artifact caused by the 30 mm polypropylene sphere in plane 4 was quantified for the different cases. In figure 8 the ASFs are plotted as a function of the distance from plane 4. As can be seen in figure 8A, the ASF is lowest for $\phi = 60°$ indicating that removal of out-of-plane blur decreases with increasing angular range. In figure 8B, there is a slightly lower ASF for $\Delta\phi = 2°$ indicating blur decreases with a smaller angle increment between each projection. Since the influence of quantum noise was sever when 31 projections were acquired it was not possible to compare the ASFs for case 3, when N_{Acq} was varied.

3.2 Tomosynthesis compared to conventional X-ray imaging

3.2.1 Exposure

To compare tomosynthesis with conventional X-ray imaging the SDNR of the investigated objects have been plotted, see figure 9. From these graphs it seems that SDNR increases much more rapidly with exposure in the reconstructed images, though how this will affect the visibility of objects is not clear.

Each of the projections were acquired with 60 kVp and different mAs. Some of the reconstructed slices are shown in figure 10 together with conventional images acquired with the same tube settings. A higher mAs increases the SDNR more with tomosynthesis, as can be seen in figure 9. In figure 10 it is easier to discern small objects in the tomosynthesis images compared to the conventional, especially those in plane 4 (z = 120 mm above the table). Even though each of the studies were acquired with the same tube settings (same kV and total mAs) it must be kept in mind that the exposure will be affected by the inverse square law due to the oblique tomosynthesis projections. Hence, to get comparable images (in terms of object visibility) a larger dose is required with the conventional technique.

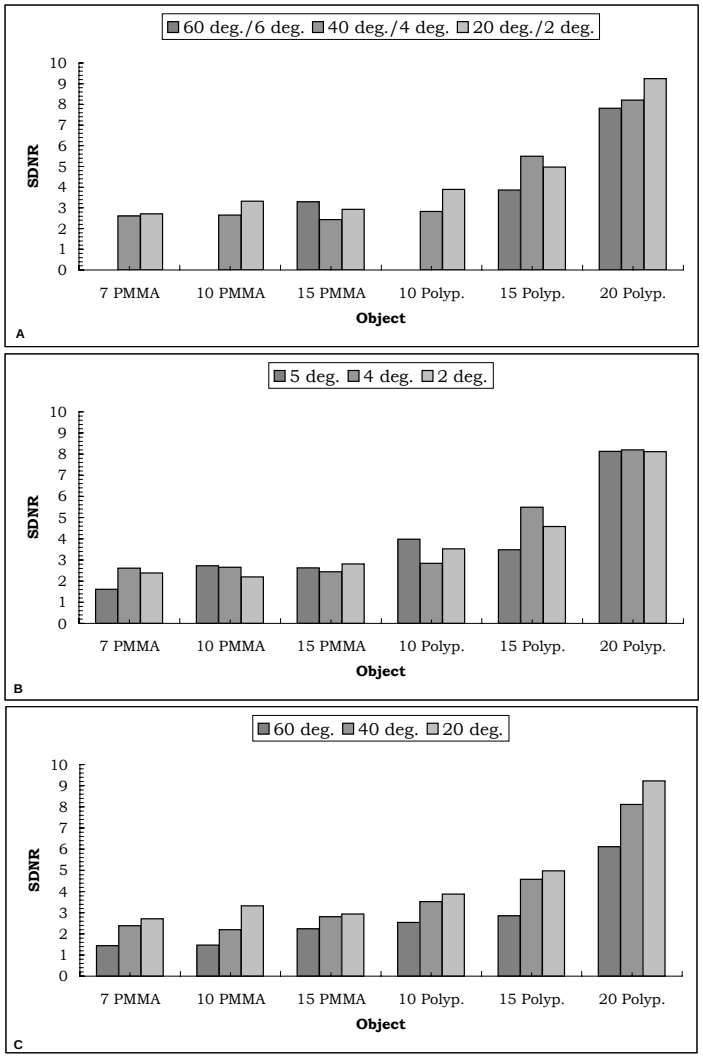

Figure 7: The graphs show how the SDNR varies with A) tomographic angle, ϕ, B) angle increment, $\Delta\phi$, and C) number of projections, N_{Acq} ($\Delta\phi = 2$). Note (in A) that objects smaller than 15 mm were not visible when $\phi = 60°$.

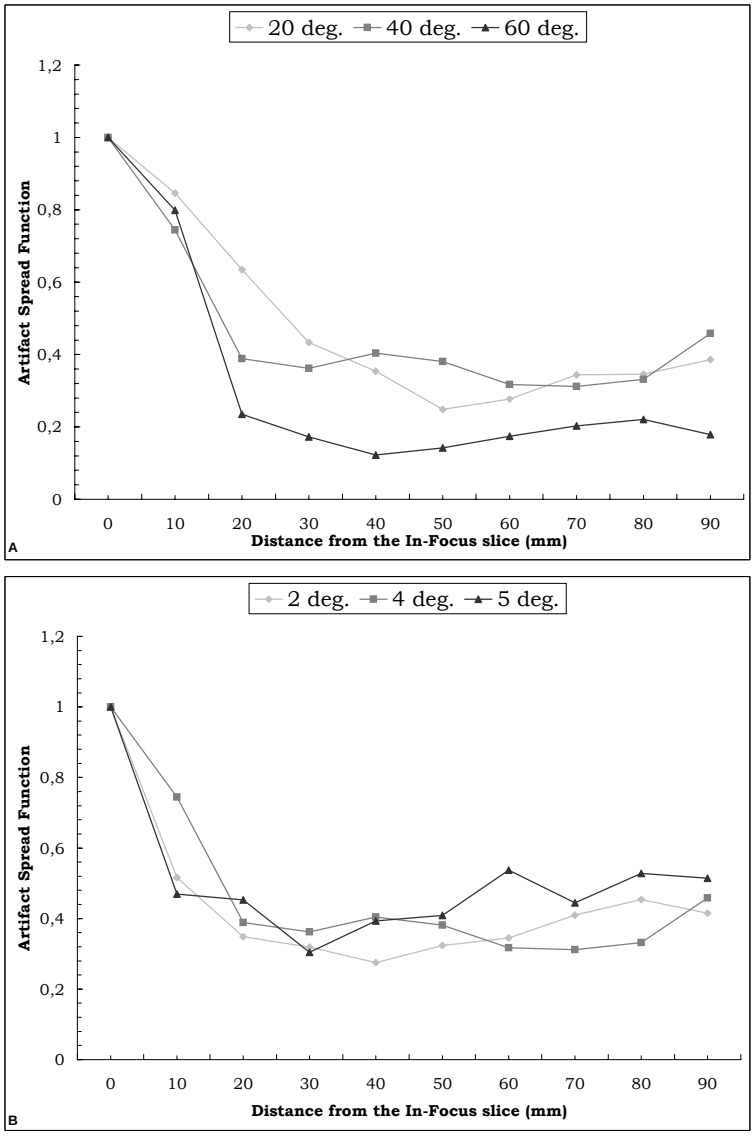

Figure 8: The artifact spread function as a function of the distance from plane 4 where the object is located. The parameter settings were; 60 kVp and 10 mAs/projection. In A) the angular range was varied ($N_{Acq} = 11$) and B) the angle increment ($\phi = 40°$).

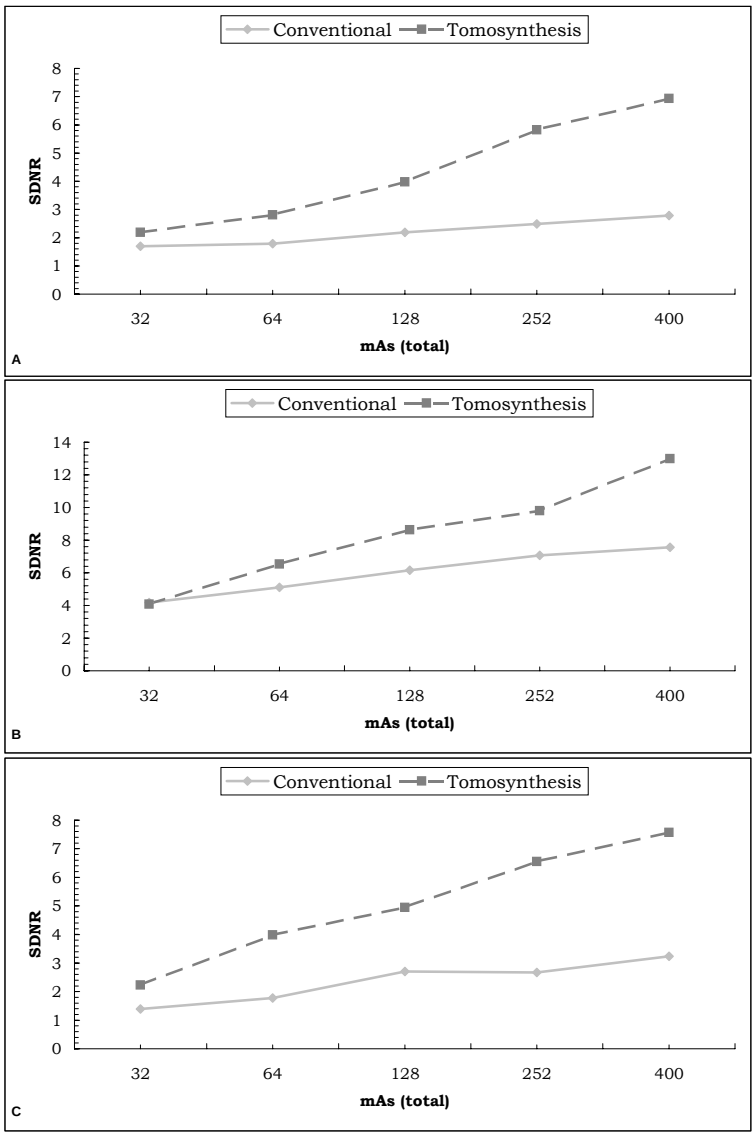

Figure 9: The SDNR variations with different mAs settings for conventional X-ray imaging and tomosynthesis. The investigated objects were; A) a 10 mm polypropylene sphere located at plane 4, B) a 20 mm polypropylene sphere located at plane 1 and C) a 15 mm PMMA ellipsoid located at plane 1 of the physical phantom. In figure 10 the different objects are marked with arrows.

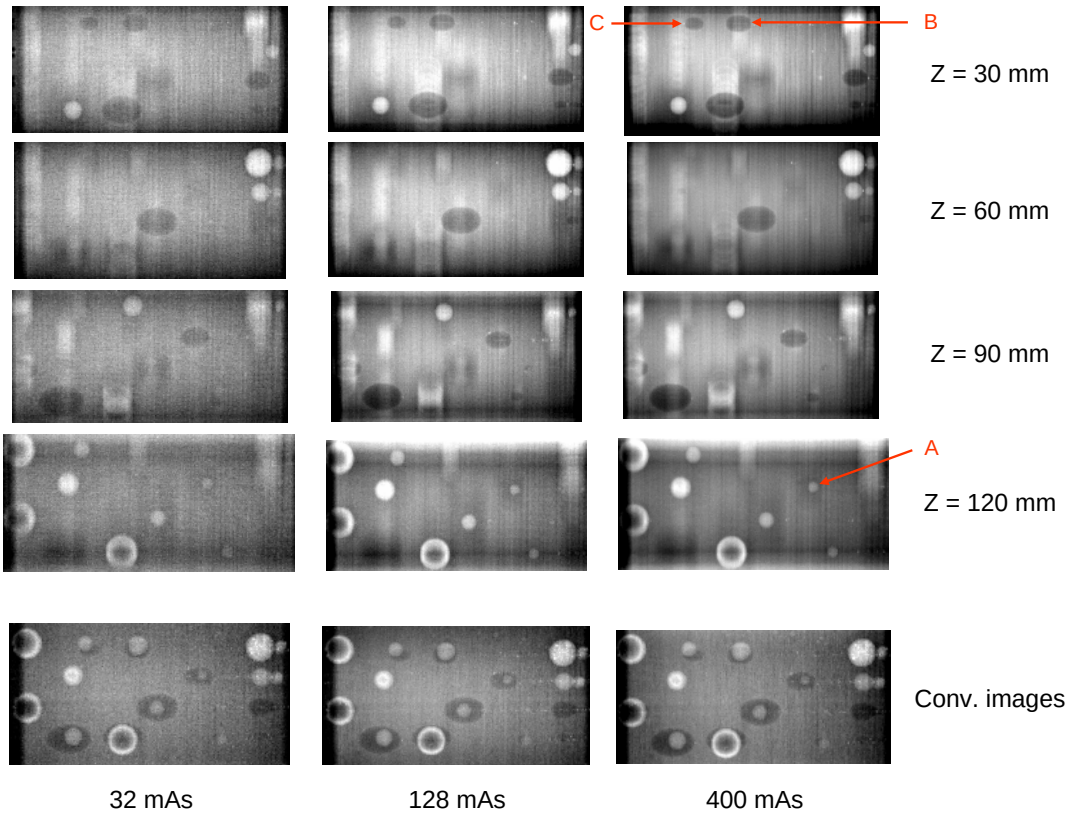

Figure 10: Slices reconstructed from 11 projections acquired with different tube loading and 60 kVp. Three different exposures are shown together with images acquired with the conventional technique. Even though there are some artifacts present in the reconstructed slices the visibility of small objects is better in the slices especially those in plane 4 (z = 120 mm above the table). The arrows indicate the objects that were investigated.

3.2.2 Anthropomorphic phantom

The anthropomorphic phantom was reconstructed with 170 slices. The fiducial markers were located at $z_{up} = 150$ mm (slice 135) and $z_{low} = 50$ mm (slice 48), which gave the distance $\Delta z = 1.2$ mm between two adjacent slices according to equation 8. Since the lung has a thickness of approximately 150 mm in the AP direction, the entire lung was covered by ∼120 slices.

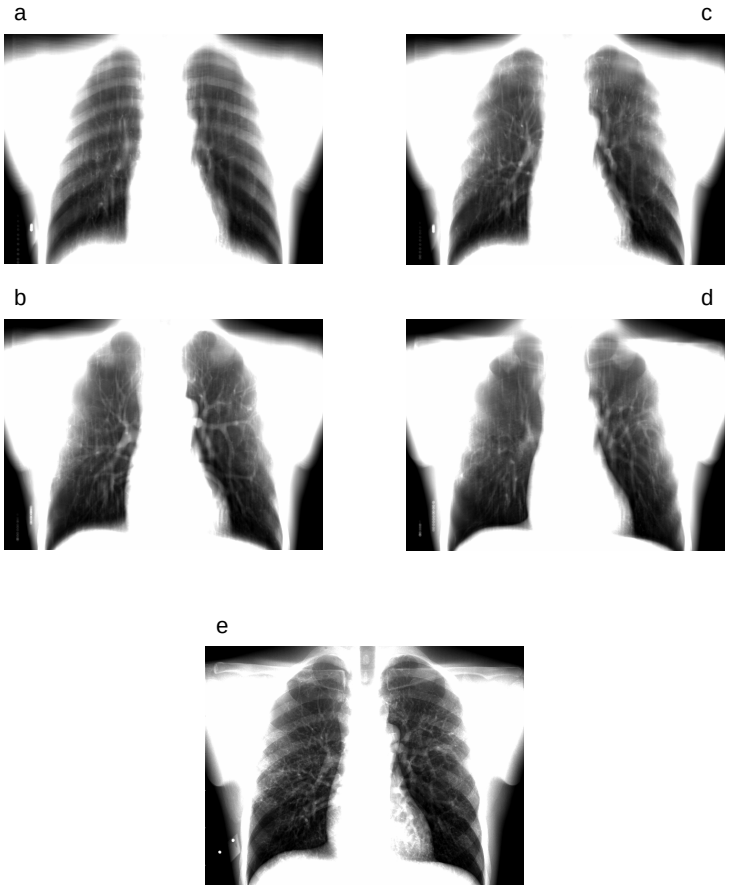

Figure 11: Reconstructed tomosynthesis planes (a - d) of the anthropomorphic chest phantom and a conventional radiograph (e). The slices are reconstructed at; a) 41 mm, b) 69 mm, c) 93 mm, d) 105 mm above the table. Each of the 11 tomosynthesis projections and the conventional AP-projection were acquired with 100 kVp and 3.2 mAs. In the reconstructed slices the ribs are blurred out and disappear when the distance from the table increase (slices in the middle of the lung).

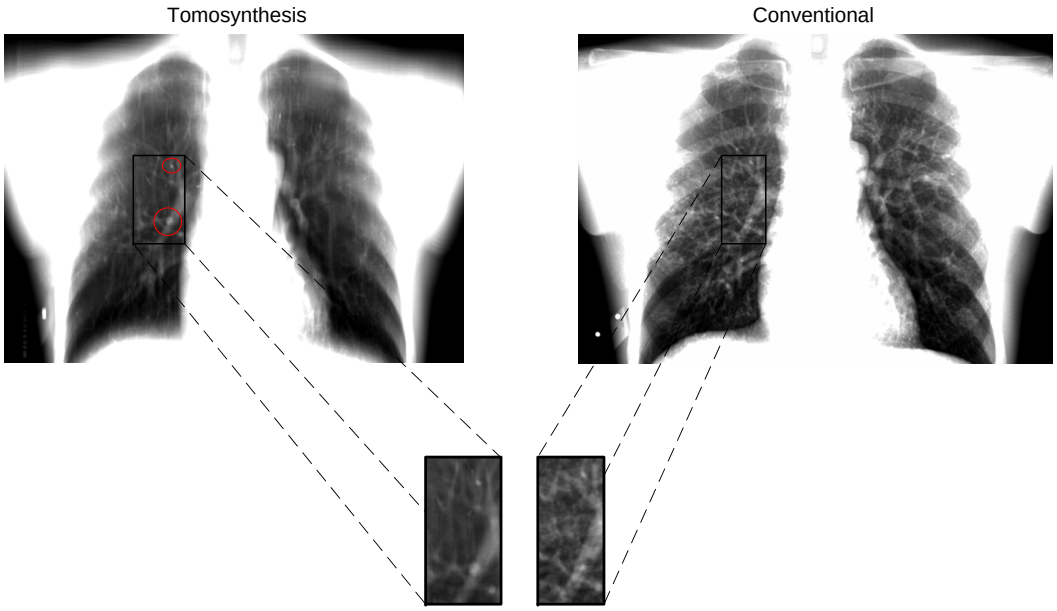

Figure 12: The tomosynthesis image show a slice located 60 mm above the table. Some small structures that are obscured in the conventional AP image are brought into focus when the overlying ribs are removed (i.e. blurred out).

In figure 11, reconstructed slices at different depths are compared to a conventional chest radiograph. With tomosynthesis object visibility is increased when the window/level is optimized for each individual slice. Another observation is that the ribs are removed (i.e. blurred out) and do not obscure objects in the middle of the lung, as they tend to do in the conventional image.

The visibility of the bronchus and some vascular structures is illustrated in figure 12. When the confusion of overlying anatomy is reduced in-focus objects are easier to discern. The SDNR is higher in the reconstructed slice and the visibility of in-focus objects is also higher. Together with depth information from equation 8 the ability to locate (pathological) structures will therefore increase with tomosynthesis compared to conventional planar X-ray images.

4 Discussion

In this thesis we have investigated some of the fundamental parameters associated with the acquisition and reconstruction in tomosynthesis. These parameters were optimized to compare tomosynthesis with conventional X-ray imaging. A clinical comparison study was also performed using an anthropomorphic chest phantom.

Tomographic parameters

The results from the investigation of the tomographic parameters indicate that the angular range (ϕ) has the greatest impact on image quality. The measured SDNR is generally lower for a larger ϕ and this is also possible to see in the images. A small angular range will improve the clarity of the objects. Some of the smallest objects were not even visible in the images reconstructed from the $\phi = 60°$ projections. This is a result of the cone beam geometry and increasing mean path length of the photons resulting in a decreased photon flux. This is also reflected in the contrast of the in-focus slices, which becomes higher as the angular range is reduced. When varying the number of projections acquired per series (with a fixed angular range) the visibility of the objects is fairly the same, independently on the number of projections acquired. The reason for this is most likely due to the fact that each of the tomosynthesis series were acquired with the same total exposure, even though the dose per projection was varied. With a smaller dose per projection the quantum noise will increase, but the dose did not vary enough to clearly visualize this effect.

The greatest advantage with tomosynthesis, compared to conventional X-ray imaging, is the possibility to reduce the influence of over- and underlying structures from an arbitrary plane in the imaged volume. But since this reduction is performed by smearing the unwanted structures over the interesting plane, the reconstructed images contain blur from out-of-plane structures. However, with the right parameter settings and reconstruction methods the blur can be minimized, which would improve visualization of valuable diagnostic information. Therefore, the most important quality factor is the capability of tomosynthesis to reduce the blur. To quantify the out-of-plane blurring created from an object in a homogenous background, the artifact spread function was measured in images acquired with different parameter settings. The graphs of the ASFs indicate that a large angular range minimizes the blurring. Moreover, the ASF also quantifies the capability of tomosynthesis to separate the reconstructed planes. Hence, less blur from overlying structures can also be interpreted as an increase in Z-resolution. In figure 6 this can be confirmed by comparing the visibility of the 30 mm ellipsoid. It is difficult to draw conclusions regarding the correlation between the projection spacing, $\Delta\phi$, (or number of projections) and the blur from the graph of the ASFs (figure 8), they are roughly the same. Intuitively, a decrease in $\Delta\phi$ leads to an increase in N_{Acq} and the exposure per projection must be adjusted accordingly (decreased to acquire the same total exposure). Therefore, objects in the in-focus plane will have a signal proportional to N_{Acq} and out-of-plane objects will have a lower signal, proportional to $1/N_{Acq}$. When adding the projections, objects outside the in-focus slice will be repeated (or smeared) over the image proportional to N_{Acq}. Hence, a larger number of projections (small $\Delta\phi$) will minimize the influence of over- and underlying structures i.e. allow reconstruction with fewer artifacts.

Some of the key results from the investigation of the tomographic parameters are summarized below.

- $\downarrow \phi \Rightarrow \uparrow$ SDNR (of in-focus objects) and $\downarrow$ Z-resolution
- $\downarrow N_{Acq} \Rightarrow \uparrow$ SDNR (of in-focus objects) and $\downarrow$ Z-resolution
- The blurring artifacts created from out-of-plane structures in the in-focus plane is a continuous effect that depends on the distance between the planes
- Since the blurring artifact is a result of overlying structures that are not separated from the in-focus plane, blur decrease as Z-resolution increase

It is important to stress that these results are just a rule of thumb, the optimal parameter setting depends on the specific situation and the composition of the anatomical surrounding. However, to minimize the influence from over- and underlying structures, which is the benefit with tomosynthesis, it is best to choose a large angular range with many projections. The angular range and the number of projections must then be balanced against the fact that for a given total examination dose, more exposures will reduce the signal for each individual projection. If the dose per projection is too low the image quality will be degraded due to receptor noise. Therefore the tomographic parameters (and exposure) must be chosen so that the SDNR of the in-focus objects is sufficient to visualize the specific structures.

Tomosynthesis compared to conventional X-ray imaging

Images were acquired with the conventional technique using five different tube loadings and five tomosynthesis series were performed with the same total tube loading. A fact that must be considered with fixed tube settings, kVp and mAs, is that the exposure will vary among the different projections due to the inverse square law. The exposure is therefore slightly lower with tomosynthesis. At the lowest exposure level the noise is high and the contrast poor, making the visibility of the smallest objects very low, for both of the modalities. As the exposure is increased the noise is reduced and objects in the in-focus slice becomes much easier to discern. Even though the exposure is fairly the same, the reconstructed tomosynthesis slices have a much better object visibility compared to the conventional images. The tomosynthesis images are even superior to conventional images acquired with a higher exposure. To improve the tomosynthesis investigation further, the dose per projection could have been weighted accordingly to the position of the tube. By using this approach the total exposure is more efficiently divided, making the outermost projections less influenced of quantum noise.

The investigated objects are much easier to discern in the reconstructed slices, for all exposure levels. The signal from an object in a specific plane is the sum of the signals from that object in all of the projections. For a high contrast object, such as the bronchus in the lungs or the spheres and ellipsoids in the physical phantom, the visibility is higher with tomosynthesis. The structures outside the in-focus plane are repeated (blurred out) in the direction of the tube movement. This will retain the high-frequency information and greatly reduce the contrast of out-of-plane structures. This is reflected in that small objects becomes visible at lower exposure with tomosynthesis. Despite the artifacts in the reconstructed images, object visibility is clearly better with tomosynthesis even with a lower dose.

The study of the anthropomorphic chest phantom showed a clinical example of the ability to visualize structures in 3 dimensions with tomosynthesis. In the anatomical images the blur

degrades the images and make the reconstructed slices fuzzy and not as crisp as the conventional image. Although, the 3D volume reconstructed with tomosynthesis had increased visibility of local structures. The reason for this is that the surrounding anatomy to an in-focus slice is smeared over the image instead of superimposed on the in-focus structures. Ribs that tend to obscure under-/overlying tissues were removed (i.e. efficiently blurred out) in the reconstructed slices which increased the contrast for some obscured objects. Laterally, where the ribs curve, visibility was increased with tomosynthesis due to improved contrast between the underlying object and the blurred-out ribs. The visibility of the bronchus and some vascular structures were increased with tomosynthesis due to the removal of overlying structures and the possibility to cut through them. Together with the depth information tomosynthesis holds the potential to improve sensitivity of pulmonary lesions over conventional X-ray imaging. This would also improve early detection of subtle lung nodules which would decrease the need for recalls. It might even be possible to discriminate between benign and malignant lesions, since the reconstructed three-dimensional volume, rather than a two-dimensional radiograph, provides information on the dimension of the lesion, on the distribution of the lesion and about the density of the lesion.

This study has focused on several parameters that affect image quality in tomosynthesis images, namely total angular range, number of projections and angular increment. The effects of these were compared using both physical measures such as SDNR as well as visual interpretation of the images. Based on visual quality assessment, tomosynthesis images benefit more from increases in dose than conventional images. Additionally, for the same doses, tomosynthesis images show increased visibility of certain structures. To confirm these results experimentally, which was beyond the scope of this thesis, clinical trials with human observers that compare images acquired with conventional X-ray images and tomosynthesis must be performed.

5 Conclusions

Compared to conventional X-ray imaging, tomosynthesis offers 3-dimensional information with increased clarity of in-focus objects due to reduced tissue overlap. The depth-resolution of the in-focus structures can be optimized by the right choice of parameter settings, with the angular range and number of projections being the most essential. But to evaluate the clinical detection and diagnostic accuracy, clinical trials will be necessary with human observers in combination with case specific optimization of the parameter settings.

6 Acknowledgements

First of all I would like to thank my supervisor Anders Tingberg for giving me the great opportunity of studying tomosynthesis and for all the help during the project. I would also like to thank Mark Ruschin for immensely helpful comments, criticisms and suggestions. Another person that have contributed a great deal for making this project possible is Magnus Båth, who provided me with the reconstruction software, thank you.

During my project in Malmö I have met many people who all have been very helpful and contributed in different ways to the project. Among these, I specially thank Peter Wallenius

for introducing me to the operational software and helping me with other practical things, together with interesting discussions. And finally I would also like to thank Mikael Gunnarsson and Marcus Hultgren for helping me with the CT acquisition and reconstruction.

References

[1] Jerrold T. Bushberg *et al.*, 2002, The Essential Physics of Medical Imaging second edition, Lippincott Williams & Wilkins

[2] Ziedses des Plantes B G, 1932, Eine neue methode zur differenzierung in der roentgenographie, Acta Radiol. 13: 182-92

[3] R. Van Tiggelen, 2002, In search of the third dimension: From radiosteroscopy to three-dimensional imaging, JBR-BTR 85: 266-270

[4] Garison JB *et al.*, 1969, Three dimensional roentgenography, Am J.Roentgenol. 105: 903-8

[5] David G. Grant, 1972, Tomosynthesis: A Three-Dimensional Radiographic Imaging Technique, IEEE Trans. On Biom. Engineering Vol. 19 No.1: 20-28

[6] Miller E R, McCurry E M and Hruska B, 1971, An Infinite Number of Laminograms from a Finite Number of Radiographs, Radiology 98: 249-55

[7] Shusuke Sone *et al.*, 1991, Development of a High-Resolution Digital Tomosynthesis System and Its Clinical Application, RadioGraphics 11:807-822

[8] James T. Dobbins III, Chest Radiography - Pt. 3: Chest Tomosynthesis, http://www.imagingeconomics.com/library/200505-05.asp

[9] Baojun Li *et al.*, 2004, The Impact of Acquisition Angular Range on the z-resolution of Radiographic Tomosynthesis, ICS 1268 13-18

[10] Tao Wu *et al.*, 2004, Digital tomosynthesis mammography using a parallel maximum-likelihood reconstruction method, Proceedings of SPIE Vol. 5368, Physics of medical imaging 1-11

[11] Devno J. *et al.*, 2003, Practical strategies for the clinical implementation of matrix inversion tomosynthesis (MITS), Proceedings of SPIE Vol. 5030, Medical imaging 379-389

[12] James T Dobbins III, Devon Godfrey, 2003, Digital Tomosynthesis: current state of the art and clinical potential, Phys. Med. Biol. 48 R65-R106

[13] Loren T. Niklasson *et al*, 1997, Digital Tomosynthesis in Breast Imaging, Radiology 205:399-406

[14] Jing Liu, Dwight Nishimura, Albert Macovski, 1989, Generalized Tomosynthesis for focusing on an arbitrary surface, IEEE Trans. Med. Imaging Vol. 8 No. 2 168-172

[15] Devon J. *et al.*, 2001, Optimization of Matrix Inverse Tomosynthesis, Proceedings of SPIE, Vol. 4320, Physics of medical imaging 696-704

[16] Bernhard E.H. Claus, Jeffrey W. Eberhard, 2002, A New Method for 3D Reconstruction in Digital Tomosynthesis, Proceedings of SPIE vol. 4684, Medical imaging 814-824

[17] Paul F. Hemler, Steve B. Robinson, 2003, Improved 3D Reconstructions For Generalized Tomosynthesis, Proceedings of SPIE Vol. 5030, Physics of medical imaging 361-370

[18] Beilei Wang, Kenneth Barner, Denny Lee, 2004, Algebraic Tomosynthesis Reconstruction, Proceedings of SPIE Vol. 5370, Medical imaging 711-718

[19] C. Badea, Z. Kolitsi and N. Pallikarakis, 2001, Image Quality in Extended Arc Filtered Digital Tomosynthesis, Acta Radiologica 42 244-248

[20] http://www.compray.com/products/canon/generaloverview/12.jpg

[21] http://www.insideinspace.com/about.html

[22] http://www.rsinc.com/

[23] Rasband, W.S., 1997-2006, ImageJ, U. S. National Institutes of Health, Bethesda, Maryland, USA, http://rsb.info.nih.gov/ij/

[24] Tao Wu *et al.*, 2004, A Comparison of Reconstruction Algorithms for Breast Tomosynthesis, Medical Physics Vol. 31 No. 9 2636-2647